

Article

Preparation and the Effect of Surface-Functionalized Calcium Carbonate Nanoparticles on Asphalt Binder

Chenchen Shen ¹, Rui Li ^{1,*}, Jianzhong Pei ¹, Jun Cai ², Tao Liu ¹ and Yang Li ¹

¹ School of Highway, Chang'an University, Xi'an 710064, China; Shenc@chd.edu.cn (C.S.); peijianzhong@126.com (J.P.); liutao@chd.edu.cn (T.L.); liiyang@chd.edu.cn (Y.L.)

² College of Traffic and Transportation Engineering, Changsha university of science and technology, Changsha 410114, China; fromhscaijun@163.com

* Correspondence: lirui@chd.edu.cn

Received: 20 November 2019; Accepted: 16 December 2019; Published: 20 December 2019



Abstract: To solve the nanoparticles (NPs) agglomeration phenomena of nanometer calcium carbonate (nano-CaCO₃) modified asphalt binder, in this paper, solvent-free CaCO₃ nanofluids (NFs) were prepared based on surface-functionalized CaCO₃ NPs to study the effect on asphalt. Microscopic structures, compositions, and thermal stability were characterized by Fourier transform infrared spectrometer (FTIR), X-ray diffractometer (XRD), transmission electron microscope (TEM), and thermogravimetric analyzer (TGA), respectively. Results showed that perfect CaCO₃ NFs were successfully prepared, and were good enough for asphalt mixing due to their excellent thermal stability. Scanning electron microscopy (SEM), conventional tests, dynamic shear rheometry (DSR), and bending beam rheometry (BBR) were conducted to investigate the modifying effect. The SEM results indicated that CaCO₃ NFs had better compatibility with asphalt binder than original CaCO₃ NPs. Conventional and DSR test results demonstrated that CaCO₃ NFs had slight negative effects on high-temperature performance while improving the low-temperature performance of the asphalt binder. The BBR test results confirmed that the modifier addition effectively enhanced asphalt binders' low-temperature crack resistance performance.

Keywords: solvent-free CaCO₃ nanofluids; microscopic structure; modified asphalt binders; compatibility; rheological performance; low-temperature creep performance

1. Introduction

The term “nanomaterial” generally refers to one comprised of particles whose characteristic dimension is between 1 and 100 nm. Due to the unique properties of nanomaterials, such as high ductility, strong surface effect, and small size, its application in asphalt binder as a modifier is very widespread at present. Previous studies showed that nanomaterials could significantly improve the performance of asphalt binder (e.g., high-temperature performance [1,2], crack resistance [3], aging resistance [4,5], fatigue resistance [6], adhesion [7,8], etc.). Therefore, nanomaterials play an increasingly important role in the study of asphalt binder modification [9,10].

However, the interfacial bonding strength between nanomaterial and asphalt binder is relatively weak due to their different interfacial properties; interfacial defects form easily between organic and inorganic materials, thus resulting in nanocomposites' performance degradation [11–13]. Some factors also increase the difficulties of dispersion and stability on the microscopic scale, such as the high viscosity of asphalt and the agglomeration of nanoparticles (NPs) with high surface energy [14,15]. Previous research found that NPs exist in the form of agglomerates or cause local enrichment or segregation due to the above problems, thus resulting in uneven microstructure of the composite material and distortion of the force field, which not only affects the normal function of the nano effect,

but also sometimes plays an opposite role [15,16]. Besides, if dispersion and compatibility are not considered, it is only possible to obtain a slight improvement in the physical and mechanical properties of the asphalt binder, and the performance may deteriorate because of poor operation. Previous studies showed that CaCO₃ NPs and nano clay improved asphalt binder's high-temperature properties, while reducing the low-temperature performance by direct addition [7,17].

Overall, the compatibility and dispersibility of nanomaterial in asphalt binder are the keys to the modified binders' excellent performance, and the ultimate goal of road researchers is to study how to adopt appropriate technological measures to mix the asphalt nanocomposite well and uniformly disperse nanomaterial in asphalt binder [10,15]. Since compatibility is a basic and necessary condition for dispersion stability, it is of great research value to develop new methods to improve nanomaterial asphalt binder compatibility.

The emergence of solvent-free nanomaterials with liquid-like behavior provided new ideas for solving the above problems, and it was reported that NPs chemically grafted with long organic molecular chains on their surface can exhibit liquid-like fluidity in solvent-free conditions [18–22]. This modification technology on the surface of nanomaterials is expected to solve the issue of agglomeration in NPs-modified asphalt binders.

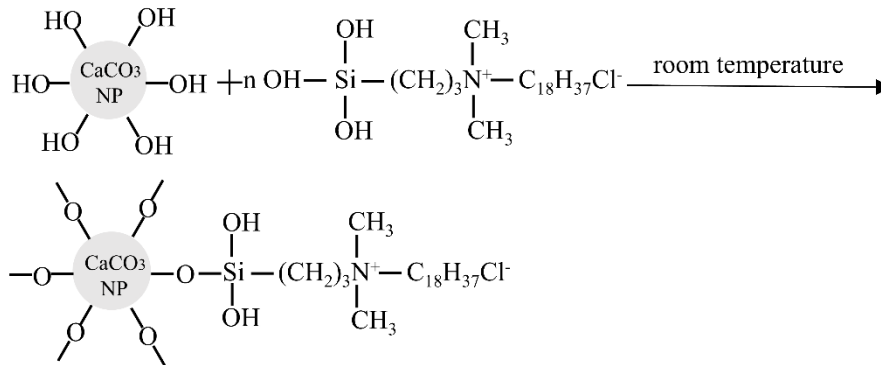
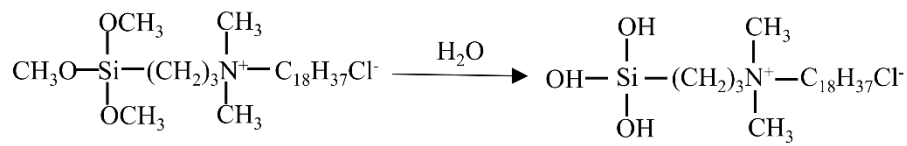
Based on previous work, in this paper, CaCO₃ nanofluids (NFs) were prepared based on CaCO₃ NPs. The main objective of this research was to study the effect of CaCO₃ NFs addition on asphalt binder. The microstructures of CaCO₃ NFs were characterized. The rheological properties of binders were evaluated through dynamic shear rheometry (DSR) and bending beam rheometry (BBR). The compatibility of CaCO₃ NFs and NPs with asphalt binder was also compared by scanning electronic microscopy (SEM). It is expected that this study can provide some research results for the application of CaCO₃ NFs in asphalt pavement.

2. Raw Materials and Preparation

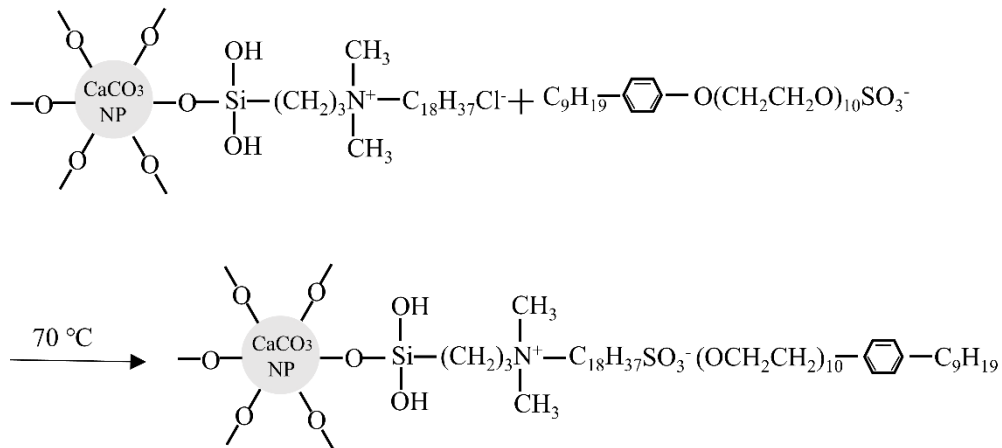
The main technical indexes of the original CaCO₃ NPs are shown in Table 1. The surface of CaCO₃ NPs were modified by chemical grafting and ion exchange techniques, and quaternary ammonium salt (CH₃O)₃Si(CH₂)₃N⁺(CH₃)₂(C₁₈H₃₇)Cl⁻ (DC5700) as well as sulfonate salt C₉H₁₉C₆H₄O(CH₂CH₂O)₁₀SO₃⁻Na⁺ (NPES) were used in this study. The details of surface chemical grafting and ion exchange were based on the methods described by Li [22], and the final target products which flowed at a lower heating temperature in the absence of any solvent were referred to as solvent-free CaCO₃ NFs. The specific reaction equations are listed as follows (Schemes 1 and 2), and the synthetic schematic diagram is shown in Figure 1.

Table 1. Properties of original CaCO₃ nanoparticles (NPs) used in this study.

Properties	Test Values
Exterior	White paste
Moisture (wt%)	50
Solid content (wt%)	50
Average particle size (nm)	50–70
Specific surface area (m ² /g)	19.2
pH	9.52



Scheme 1. Grafting of coupling agent reaction.



Scheme 2. Ion exchange reaction.

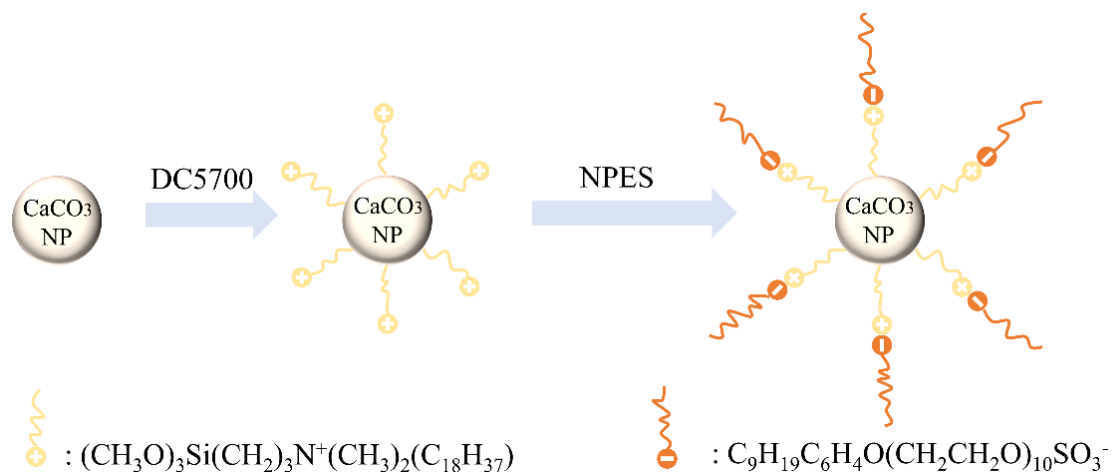


Figure 1. Schematic diagram for synthesis of CaCO₃ nanofluids (NFs).

Correspondingly, Table 2 shows the basic parameters of 90# base asphalt binder purchased from SK company (SK-90) used in this work. The requirement refers to the regulations of the Ministry of Transport (MOT) in 2004. While preparing CaCO₃-NFs-modified asphalt binders, base asphalt

binder was heated to a flowable state in an oven, placed in a constant-temperature oil bath at 160 °C, and then blended with the CaCO₃ NFs addition by mechanical stirring for a period of time. The dosage of modifier was varied from 1% to 5%. To compare the compatibility of nano-CaCO₃ before and after surface modification with asphalt binder, 5% CaCO₃-NPs-modified binder was prepared by the same methods.

Table 2. The basic parameters of the base asphalt binder.

Technical Index	Values	Requirement (MOT, 2004)
Penetration (25 °C, 0.1 mm)	81.8	80–100
Ductility (15 °C, cm)	128.1	≥100
Softening Point (°C)	46.2	≥45
Density (15 °C, g/cm ³)	1.002	≥0.995
Solubility (trichlorethylene)/%	0.16	≤±0.8

3. Experimental Plan

3.1. Microscopic Structure Tests of CaCO₃ NFs

In this section, microscopic structure tests were conducted to verify the successful preparation of CaCO₃ NFs and their suitability as asphalt binder modifier. The products in each stage were characterized by Fourier transform infrared spectrometer (FTIR), and the samples were prepared by KBr mode. The crystal structure changes during the reactions were investigated by X-ray diffractometer (XRD). CaCO₃ NFs' thermal stability was evaluated by a comprehensive thermogravimetric analyzer (TGA) in the range from room temperature to 800 °C under nitrogen atmosphere, and the heating rate was 10 °C/min. After the samples were ultrasonically dispersed in absolute ethanol, the microstructure changes of nano-CaCO₃ before and after grafting organic matter were further observed by transmission electron microscopy (TEM).

3.2. Performance Evaluation of Asphalt Binders

3.2.1. Compatibility Performance

The experimental methods for studying the modified asphalt binders' compatibility performance are based on blending theory. Previous research used SEM to observe the modified asphalt binders' morphology, and characterized the distribution and fineness of the polymers in asphalt binder [23,24]. A blending system with better compatibility has a finer particle size when the blending process is the same, and the reduction of the dispersed phase's particle size could be an important index for improving the compatibility. In this section, SEM was conducted to compare the compatibility of asphalt binders modified with CaCO₃ NPs and NFs.

3.2.2. Conventional Performance

To test the basic performance index of the asphalt binder, the penetration at 25 °C was measured by a LZY-50A asphalt penetration meter, the ductility at 5 °C was measured by an LYY-8 asphalt tensile testing machine, and the softening point was measured by HDLR-IV. The tests were conducted in accordance with ASTM D5, ASTM D113, and ASTM D36, respectively.

3.2.3. Rheological Properties

DSR was originally developed to evaluate the viscoelasticity of asphalt binder, and the binder's dynamic rheological performance was estimated by DSR testing in this work [25–27]. In many previous studies, DSR testing has been used to evaluate asphalt binders' high- and low-temperature performance [28–34]. In this paper, DSR tests were conducted using a Smart Pave 102 DSR rheometer (Anton Parr). A sinusoidal shear load was applied to the asphalt samples, and the maximum shear strain

level was controlled at 10%. Considering that this section aimed to study the asphalt binder's high- and low-temperature performance under the effects of CaCO_3 NPs modification, dynamic frequency sweep (FS) and high-temperature sweep (TS) were performed separately to analyze the effect of modifier on the dynamic complex modulus ($|G^*|$), phase angle (δ), and the calculated high-temperature rutting factor ($|G^*|/\sin \delta$). The high-temperature FS tests were conducted at 28, 40, 52, 64, and 76 °C, with a test plate diameter of 25 mm and plate gap of 1 mm. The TS tests' temperature ranged from 30 to 80 °C, increased by 5°C/min. Correspondingly, the low temperatures were 12, 0, and −12 °C, and the plate diameter and plate gap were 8 mm and 2 mm, respectively.

3.2.4. Low-Temperature Creep Properties

BBR was originally proposed to evaluate the low-temperature creep performance of asphalt binder, and many achievements have been made using BBR tests [35–37]. In this section, the BBR used was manufactured by Cannon Company, and the tests were conducted in accordance with ASTM D6648 [38]. The asphalt binders after rotating thin-film oven test (RTFOT) and pressure aging vessel (PAV) were taken for tests, respectively, to simulate the heat aging during the construction process and the asphalt pavement after aging for at least 5 years, which mainly tested the low-temperature creep stiffness (S) and creep rate (m). The test temperatures were −12, −18, and −24 °C, and two parallel specimens were taken for each working condition.

4. Results and Discussion

4.1. Microscopic Characterization of CaCO_3 NFs

4.1.1. FTIR Analysis

Figure 2 presents the infrared spectrum of the original CaCO_3 NPs, CaCO_3 NPs grafted DC5700, and CaCO_3 NFs. In curve A, the absorption peaks at 1456 cm^{-1} , 875 cm^{-1} , and 713 cm^{-1} correspond to the stretching and bending vibration of Ca–O bond, which is a characteristic group of calcite-type CaCO_3 . Curve B had strong absorption peaks at 2924 cm^{-1} and 2854 cm^{-1} with respect to curve A, corresponding to the stretching vibration peak of C–H in methyl and methylene, respectively. Strong multiple absorption peaks appeared in the range from 1130 cm^{-1} to 1028 cm^{-1} , corresponding to the absorption peaks of Ca–O–Si bonds, indicating that the DC5700 was successfully grafted onto the CaCO_3 NPs' surface. Compared to curve B, new absorption peaks appeared at 1511 cm^{-1} , 1580 cm^{-1} , and 1610 cm^{-1} in curve C, corresponding to the skeleton vibration of the benzene ring. The stretching vibration absorption peak of RSO_4^- (NPES) appeared at 1249 cm^{-1} , showing that the anion exchanges between NPES and DC5700 were successful. In addition, the curves were gradually broadened from A to C at 1456 cm^{-1} , indicating that there were chemical interactions at each reaction stage rather than simple physical blending. In summary, the CaCO_3 NPs' surface was grafted with long-chain organic compounds DC5700 and NPES.

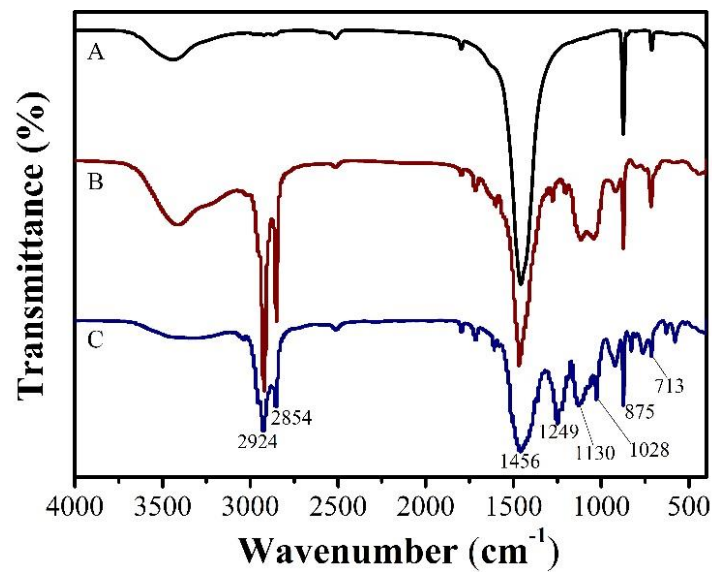


Figure 2. FTIR spectra: (A) original CaCO_3 NPs; (B) CaCO_3 NPs grafted DC5700; (C) solvent-free CaCO_3 NFs.

4.1.2. XRD Analysis

Figure 3 demonstrates the XRD pattern of original CaCO_3 NPs and solvent-free CaCO_3 NFs. The characteristic diffraction peaks appeared in both curves at 23.12° (012), 29.50° (104), 35.97° (110), 39.49° (113), 43.26° (202), 47.60° (018), and 48.59° (116) by comparing the PDF standard card (PDF NO.05-0586). The results not only suggest that the nano- CaCO_3 used in this study was calcite type, but also indicate that the surface modification of the liquid-like behavior technology did not destroy the CaCO_3 NPs' crystal structure. Additionally, curve B had some new weak diffraction peaks around 20° , indicating that there were substances with amorphous structure in addition to calcite nano- CaCO_3 . Context analysis suggests that this material was a chemical long-chain DC5700 and NPES organic substance.

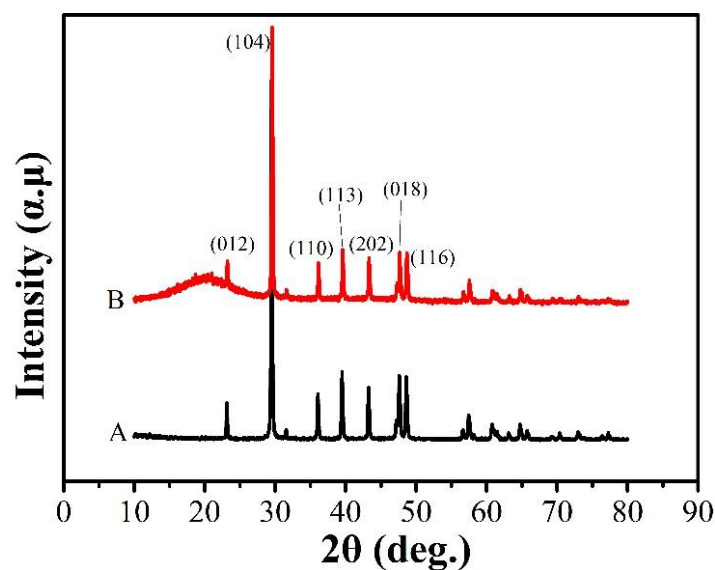


Figure 3. XRD pattern: (A) original CaCO_3 NPs; (B) solvent-free CaCO_3 NFs.

4.1.3. Morphological Analysis

Figure 4 presents macroscopic images of the prepared CaCO_3 NFs placed in a transparent glass vessel before and after heating. The NFs shown in Figure 4A exhibited a white waxy morphology at room temperature and had a certain viscosity. When slightly heated for several minutes, the NFs presented evident fluidity at about 60°C , as shown in Figure 4B–D.

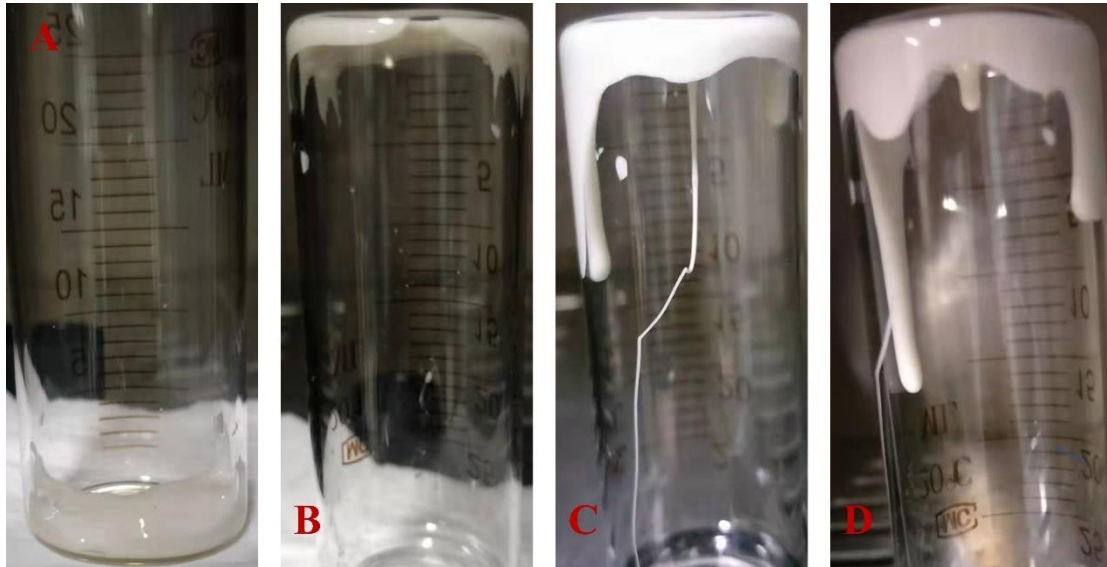


Figure 4. Macroscopic images of solvent-free CaCO_3 NFs: (A) at room temperature; (B–D) heated for several minutes at about 60°C .

Figure 5 shows TEM images of the original CaCO_3 NPs. As shown in Figure 5A, the CaCO_3 NPs' shape was cubic, and the particle size was about 50 nm. From high-resolution Figure 5B, the lattice stripes of CaCO_3 NP extended to its edge. In other words, there was no organic phase on the CaCO_3 NPs' surface.

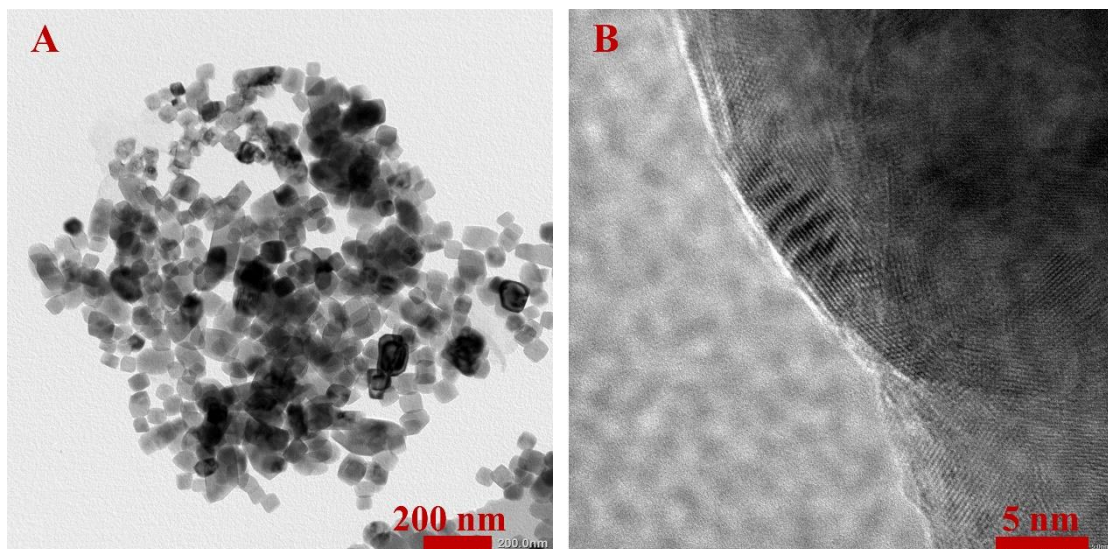


Figure 5. (A,B) High-resolution TEM images of original CaCO_3 NPs at different magnifications.

Figure 6A,B shows TEM images of CaCO_3 NFs. The figure shows that the CaCO_3 NF's surface was wrapped in a shell structure formed by organic matter, and the thickness of the shell was about 5.6 nm, which was close to the theoretically calculated thickness of organic matter layer 5.9 ± 0.4 nm [39].

It was reported that this organic matter layer provided CaCO_3 NPs with cohesive and slip-like properties that acted as a “solvent phase” in the system, giving the system a certain viscosity and fluidity [22]. Moreover, the layer firmly grafted on the nanoparticles’ surface by the chemical bonds’ action, thus ensuring that the system cannot be separated by physical effects. Figure 6C shows the scanned energy spectrum of CaCO_3 NFs in Figure 6A. The presence of Ca, C, O, Si, and S elements once again demonstrated that DC5700 and NPES were successfully grafted on the CaCO_3 NPs’ surface.

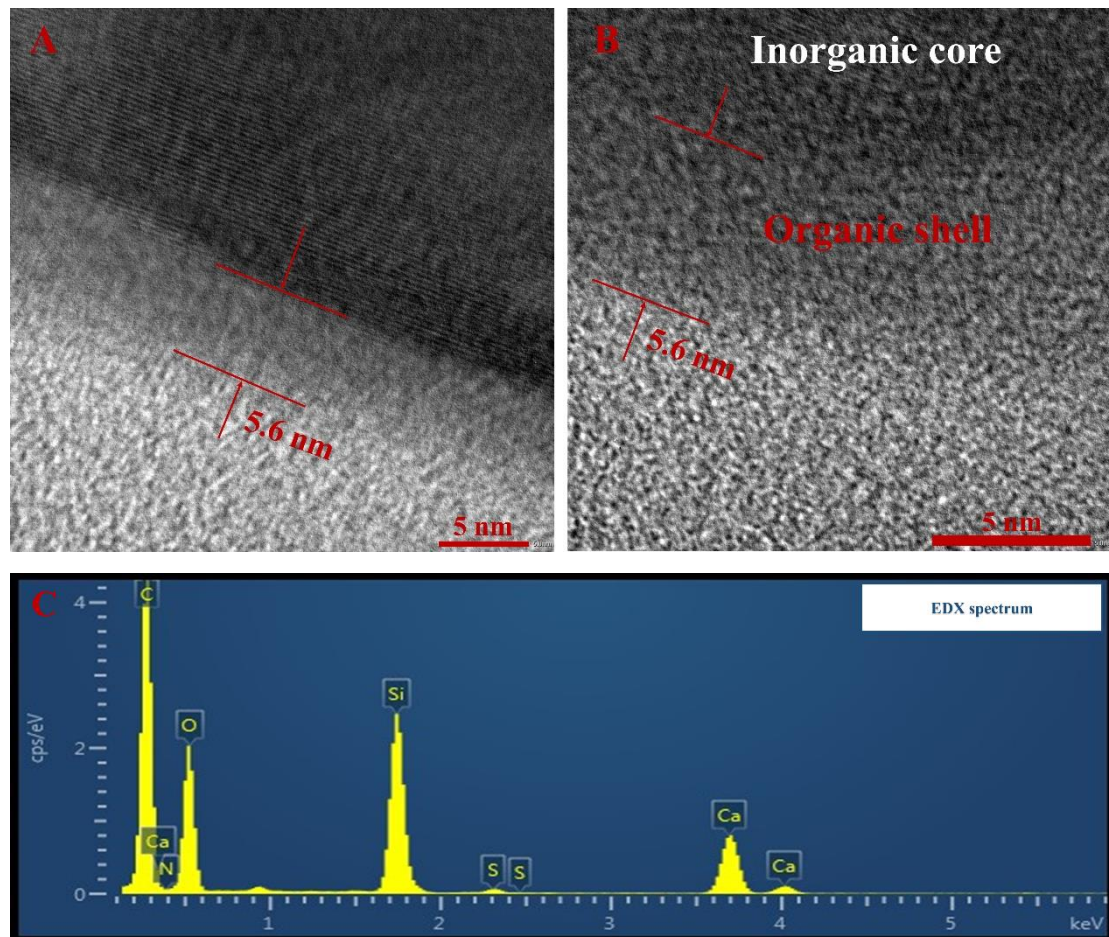


Figure 6. (A,B) TEM images of solvent-free CaCO_3 NFs; (C) EDX spectrum in (A).

4.1.4. Thermal Stability Analysis

Thermogravimetric (TG) and differential scanning calorimetry (DSC) curves of CaCO_3 NFs are illustrated in Figure 7. The thermal weight loss behavior could be roughly divided into the following stages. From room temperature to about 200 °C, the loss of mass was mainly due to the volatilization of small molecular substances in the sample, and the mass loss was within 1%, indicating that the prepared CaCO_3 NFs had higher purity. Below 150 °C, the weight was almost unchanged, indicating the solventless nature of the system. The thermal decomposition of the long-chain organic compounds DC5700 and NPES grafted on the CaCO_3 NPs’ surface was at about 200–600 °C, and the weight loss rate was about 55%, representing the organic content in the CaCO_3 NFs. Above about 600 °C, the CaCO_3 NPs were thermally decomposed. The above analysis reflects that the CaCO_3 NFs’ high thermal resistance provides the feasibility for the modified asphalt binders’ preparation at conventional temperature.

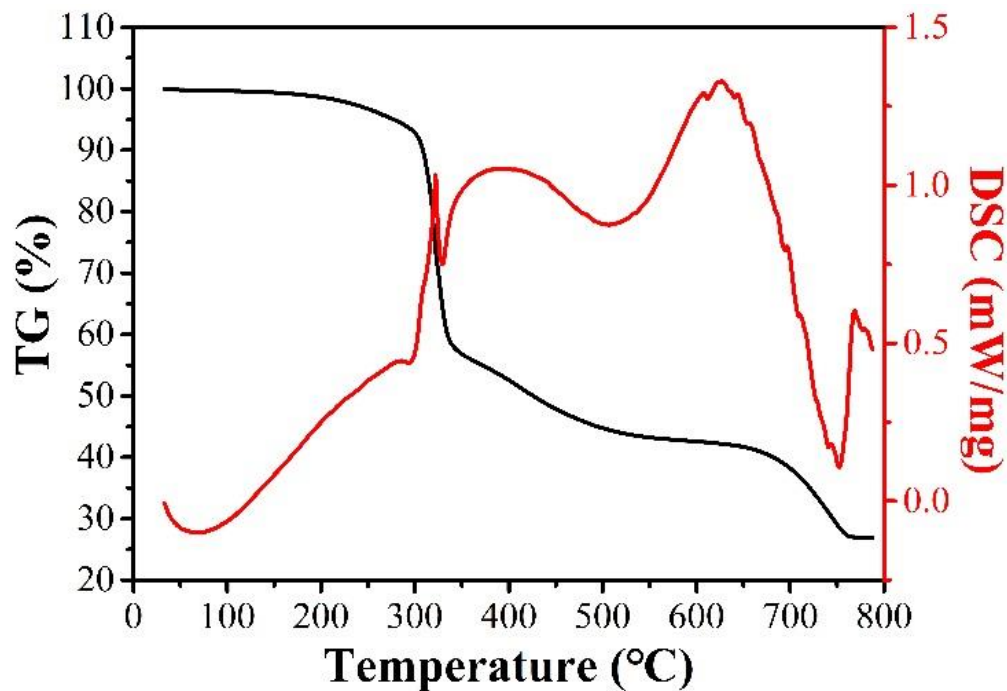


Figure 7. TG and DSC curves of solvent-free CaCO₃ NFs.

4.2. Performance of Asphalt Binders

4.2.1. Polymer Phase Morphology

Figure 8A–E shows the SEM images of CaCO₃ NPs, CaCO₃ NFs, base asphalt binder, 5% CaCO₃-NPs-modified asphalt binder, and 5% CaCO₃-NFs-modified asphalt binder, respectively. As clearly seen from Figure 8A,B, the agglomeration phenomena of the CaCO₃ NPs were severe, and there were a large number of voids, which became dense after surface functionalization.

As evident in Figure 8D, the agglomeration of the CaCO₃ NPs in asphalt binder was very obvious regardless of the high or low magnification compared with Figure 8C. The main reason for this was that the surface energy of CaCO₃ NPs was relatively high, which led to the strong interaction between particles and the consequent formation of agglomeration [40,41]. In addition, many NPs were substantially embedded in the surface of the asphalt binder rather than deeper into it. This can be explained by the fact that the interface bonding force between CaCO₃ NPs and asphalt binder is weak, the compatibility is poor, and interface defects between organic and inorganic phases are easily formed. Compared with Figure 8D, in Figure 8E, CaCO₃ NFs basically exhibited nano-scale dispersion in asphalt binder after stirring, and formed a stable blending system with asphalt binder, which had no agglomeration phenomenon and showed a more uniform dispersion effect. It can also be observed that the CaCO₃ NFs were almost entirely embedded in asphalt binder.

These results suggest that the compatibility of the CaCO₃-NFs-modified binders was better, and the interfacial force was stronger. This was mainly due to the following reasons. On the one hand, the surface energy of the nano-CaCO₃ was lowered, thus increasing the mutual repulsion among the particles. Therefore, the agglomeration weakened, and the dispersion uniformity improved. On the other hand, the organic material on the CaCO₃ NFs' surface had better fluidity, and the compatibility with asphalt binder was also better, further promoting the dispersion therein.

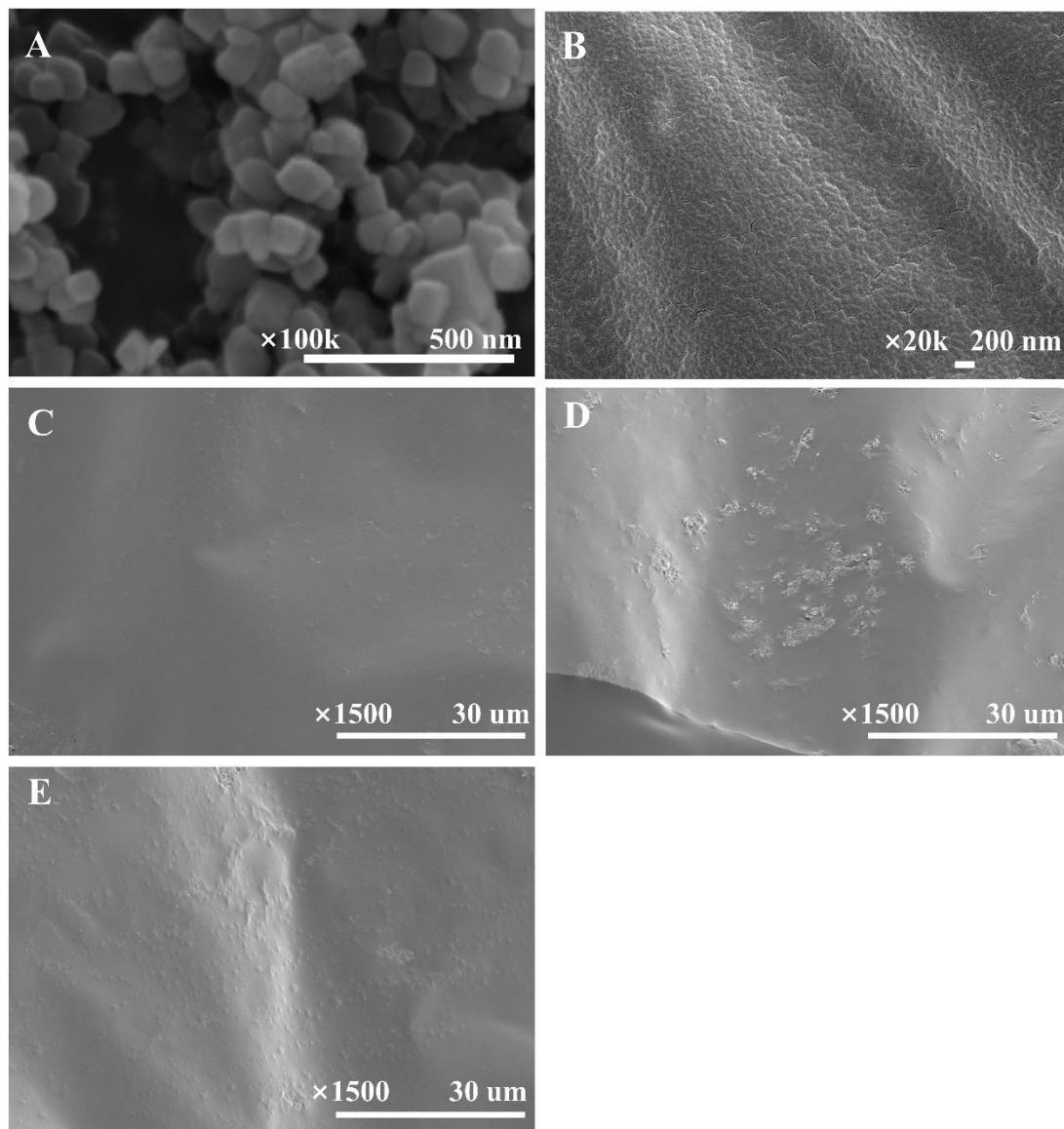


Figure 8. SEM microstructure images: (A) CaCO₃ NPs; (B) CaCO₃ NFs; (C) base asphalt binder; (D) 5% CaCO₃-NPs-modified asphalt binder; (E) 5% CaCO₃-NFs-modified asphalt binder.

4.2.2. Conventional Properties Analysis

In this paper, the conventional tests of asphalt binder properties included penetration at 25 °C, softening point, and ductility at 5 °C, and the results are shown in Table 3. The CaCO₃ NFs addition increased the ductility, indicating that the low-temperature performance of asphalt binder was improved to a certain extent. However, the addition slightly increased the penetration and decreased the softening point, indicating that the high-temperature performance of the asphalt binder was negatively affected. In summary, the results preliminarily suggest that the CaCO₃ NFs had a negative effect on the asphalt binder's resistance to rutting performance, while they improved the low-temperature crack resistance.

Table 3. Test results for three key parameters of the asphalt binders.

Test Items	Dosage (%)			
	0	1	3	5
Penetration (25 °C, 0.1 mm)	81.8	82.1	82.9	83.0
Ductility (5 °C, cm)	7.4	8.9	10.8	12.0
Softening Point (°C)	46.2	45.9	45.8	45.1

4.2.3. DSR Test

The $|G^*|$ and δ were obtained from the five temperatures by high-temperature FS. Based on the time–temperature superposition, master curves were constructed for four kinds of asphalt binders (Figure 9). Overall, the curves have similar shapes and trends. As can be seen from Figure 9a, $|G^*|$ increased as the reduced frequency increased, and the control binder had higher $|G^*|$ compared to the others. In other words, the addition of the CaCO_3 NFs caused a slight decrease in the $|G^*|$. It can be explained by the fact that the CaCO_3 NFs begin flowing with the increasing temperature, which softens the texture of asphalt binder, thus reducing the overall high-temperature stiffness of the asphalt binder. In Figure 9b, the δ gradually decreased with increasing reduced frequency. When the reduced frequency and CaCO_3 NFs content increased continuously, the δ decreased, and the δ values' gap gradually increased. This indicates that the modifier addition reduced the viscous component of the modulus under load, and increased the portion of the recoverable deformation.

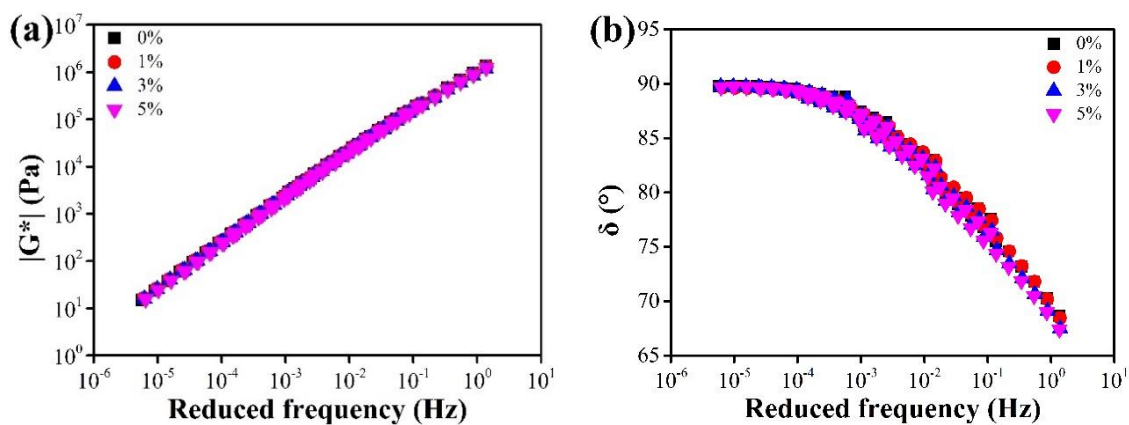


Figure 9. Master curves of asphalt binders at 28–76 °C: (a) $|G^*|$; (b) δ .

The $|G^*|/\sin \delta$ is an index of the high-temperature stability of asphalt binder, and a higher $|G^*|$ and lower δ indicate a better resistance to rutting performance. The asphalt binders' $|G^*|/\sin \delta$ values at five temperatures and test frequencies were calculated, as detailed in Figure 10. Overall, the $|G^*|/\sin \delta$ increased with increasing frequency, and decreased with increasing temperature. Further observations found that the modifier addition caused the $|G^*|/\sin \delta$ to decrease slightly, and the influence gradually weakened as the temperature increased. Taking the above analysis into consideration, the CaCO_3 NFs had a slight negative effect on the high-temperature performance of asphalt binder.

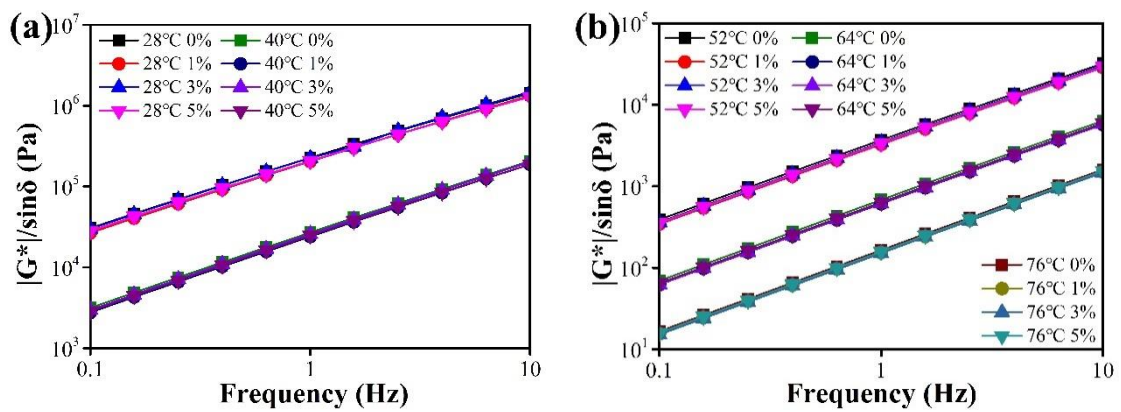


Figure 10. High-temperature rutting factor $|G^*|/\sin \delta$ of asphalt binders at: (a) 28, 40 °C; and (b) 52, 64, and 76 °C.

High-temperature TS test results still showed similar changing trend of the four binders, as shown in Figure 11. With increasing temperature, the $|G^*|$ and δ gradually decreased and increased, respectively. The $|G^*|$ decreased with increasing modifier content, but the influence was not obvious. In the temperature range of 30–50 °C, the δ values' gap increased with the increasing content, and the gap reduced gradually as the temperature increased, corresponding to the changes in the FS test. Besides, the trend of the $|G^*|/\sin \delta$ was similar to that for $|G^*|$. In summary, the results of the TS tests were similar to the above FS test, further confirming that the modifier slightly reduced the asphalt binder's resistance to rutting performance.

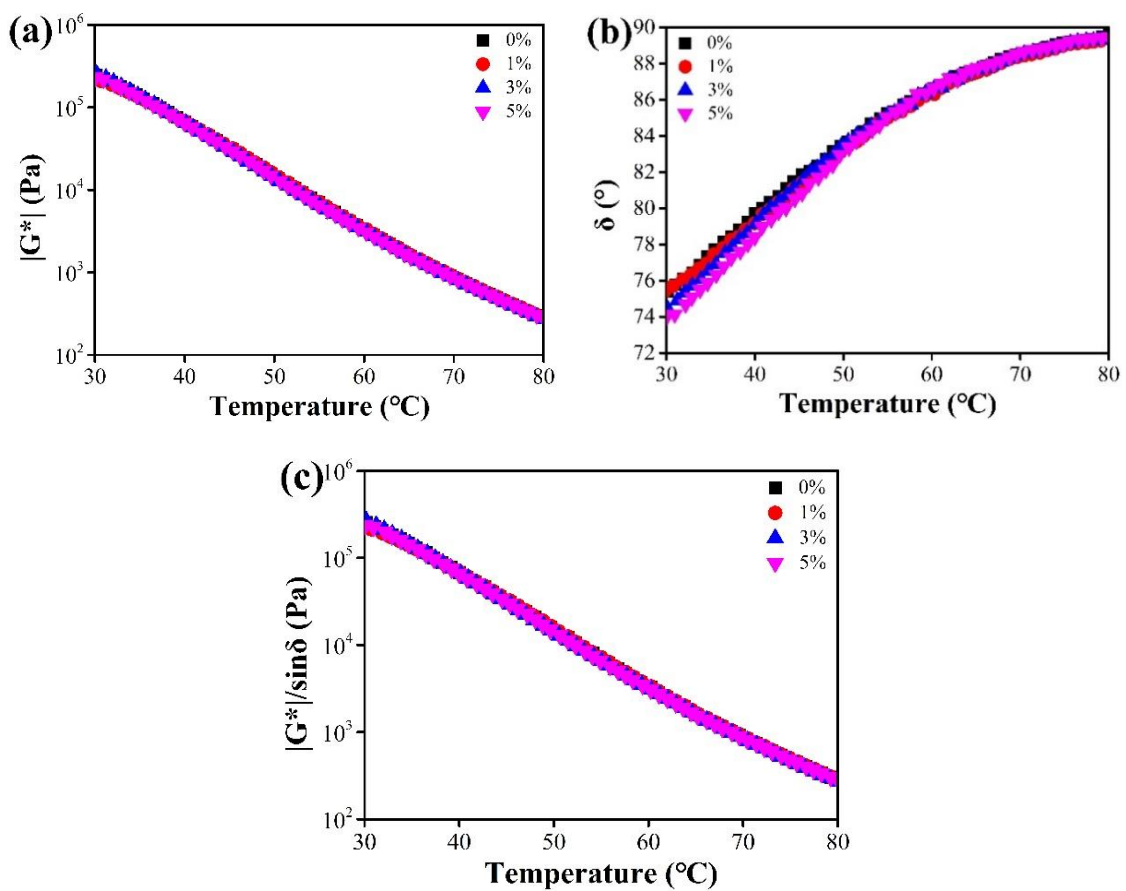


Figure 11. Temperature sweep of asphalt binders at 30–80 °C: (a) $|G^*|$; (b) δ ; (c) $|G^*|/\sin \delta$.

Similarly, the $|G^*|$ and δ were obtained from the three temperatures by low-temperature FS. As mentioned earlier, based on the time–temperature superposition, master curves were constructed for the asphalt binders, and are plotted in Figure 12. The minimum $|G^*|$ and maximum δ generally appeared at the maximum frequency. As shown in Figure 12a, the $|G^*|$ increased as the reduced frequency increased. Regarding the effect of modifier addition, the modified binders had lower $|G^*|$ than the control binder, and the changes gradually became more obvious with increasing modifier content and reduced frequency. This is mainly due to the lower brittle point of the CaCO_3 NFs, softening the texture of asphalt binder, and thus reducing the overall stiffness of binders and improving the resistance to tensile deformation at low temperature. As illustrated by Figure 12b, on the whole, the δ dropped as the reduced frequency increased. When the reduced frequency increased, the δ values' gap among the four asphalt binders increased gradually with the increasing modifier content. This indicates that the modifier addition increased the asphalt binder's viscous portion, which improved the flexibility of the asphalt binder, thus enhancing the resistance to cracking at low temperature. The above analyses suggest that the addition of CaCO_3 NFs could improve the asphalt binder's low-temperature performance, especially at lower temperatures, and the effect was more evident with increasing modifier content.

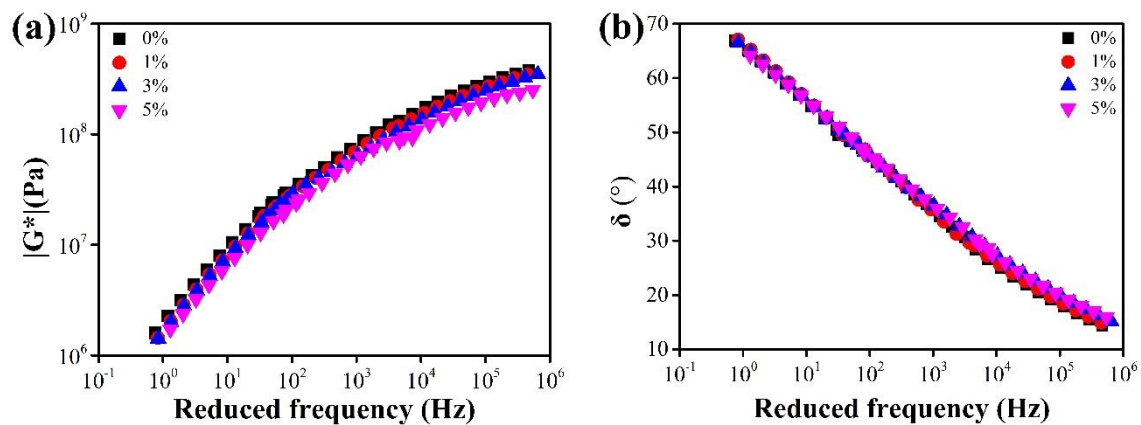


Figure 12. Master curves of asphalt binders evaluated at temperatures ranging from 12 to -12 °C: (a) $|G^*|$; (b) δ .

4.2.4. BBR Test

The values of asphalt binders' S and m are displayed in Figure 13 at three temperatures. The results showed similar trends for all four binders. The S and m increased and decreased, respectively, as the temperature decreased. Besides, compared with short-term aging, the S increased after long-term aging, while the m decreased.

In Figure 13a, the modified binders' S values were lower than the control binder under the same freeze–thaw cycle conditions, especially at -24 °C, and the S decreased gradually with the increase of the modifier content. This indicates that the low-temperature flexibility and resistance to deformation of the control binder reduced more significantly than the modified binders as the temperature decreased, especially at low temperatures (below -20 °C), and the impact was more remarkable as the modifier dosage increased.

From Figure 13b, the modified binders' m values were generally higher than the control binder under the same freezing and thawing temperature, and the values' gap was more evident at -18 °C. Overall, the greater the modifier content, the greater the m value. These results suggest that the modified binders' stress relaxation and low-temperature cracking performance were better than the control binder as the pavement temperature decreased, and the effect gradually became more obvious as the modifier content increased.

Taking the above analyses into consideration, the BBR test results further confirmed that the addition of CaCO₃ NFs improved the low-temperature cracking performance of the asphalt binder. In detail, the low-temperature crack resistance performance related to NFs addition was ranked as: 5% > 3% > 1% > 0%.

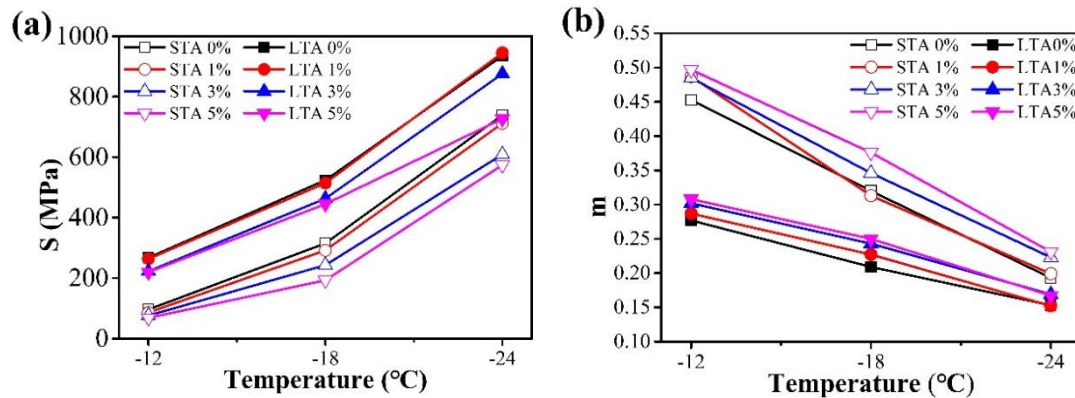


Figure 13. Low-temperature bending rheological parameters of short-term aged (STA) and long-term aged (LTA) asphalt binders: (a) creep stiffness modulus; (b) creep rate.

5. Conclusions

In this paper, solvent-free CaCO₃ NFs and modified asphalt binders were prepared based on CaCO₃ NPs. Through the tests of CaCO₃ NFs' microstructure and properties, as well as the modified asphalt binders' performance, the main conclusions can be summarized as follows.

- (1) The results of microstructural characterization proved that the CaCO₃ NFs were successfully prepared. Besides, the TG-DSC test confirmed that they were good enough to be applied in the asphalt binder at conventional temperatures due to their excellent thermal stability.
- (2) After the CaCO₃ NFs addition, for modified asphalt binders, the penetration and softening point increased, and the ductility obviously increased, indicating that the high-temperature performance was negatively affected and the low-temperature performance was improved with the addition of CaCO₃ NFs.
- (3) The effects of CaCO₃ NFs addition on rheological properties were investigated by DSR tests. The addition had a slight negative effect on the high-temperature properties of asphalt binder. However, the positive influence at low temperatures was rather evident, especially at lower temperature (i.e., below −20 °C).
- (4) The BBR tests further confirmed that the addition of CaCO₃ NFs enhanced the low-temperature cracking performance of the asphalt binder, and the influence gradually became more obvious with the increase of the modifier percent at temperatures below −12 °C. However, further research is needed to determine the optimal amount.
- (5) SEM observation indicates that the compatibility with asphalt binder was improved after chemically grafting the surface of the CaCO₃ NPs into CaCO₃ NFs. Compared with the 5% CaCO₃ NPs addition, the same dosage of CaCO₃ NFs showed better compatibility with asphalt binder.
- (6) The CaCO₃ NFs addition provides new ideas for the better application of original nanomaterials in asphalt binder. However, based on the content of each component in the CaCO₃ NFs, the price required was about three times that of the original CaCO₃ NPs at the same weight. Moreover, the energy consumption during the complicated preparation process also increased costs, so inexpensive production technology is required for further development.

Author Contributions: Conceptualization, R.L. and J.P.; Formal analysis, T.L. and Y.L.; Methodology, C.S., R.L. and J.C.; Supervision, R.L. and J.Z.; Validation, C.S. and R.L.; Writing—original draft, C.S.; Writing—review & editing, C.S. All authors have read and agreed to the published version of the manuscript.

Funding: This research was funded by [the Special Fund for Basic Scientific Research of Central College of Chang'an University] grant number [Nos. 300102219316 and 300102219308]. The authors gratefully acknowledge their financial support.

Conflicts of Interest: The authors declare no conflict of interest.

References

1. Khattak, M.J.; Khattab, A.; Rizvi, H.R.; Zhang, P. The impact of carbon nano-fiber modification on asphalt binder rheology. *Constr. Build. Mater.* **2012**, *30*, 257–264. [[CrossRef](#)]
2. Amirkhani, A.N.; Xiao, F.P.; Amirkhani, S.N. Evaluation of high temperature rheological characteristics of asphalt binder with carbon nano particles. *J. Test Eval.* **2016**, *39*, 1–9.
3. Yang, Z.; Hollar, J.; Shi, X. Surface-sulfonated polystyrene microspheres improve crack resistance of carbon microfiber-reinforced Portland cement mortar. *J. Mater. Sci.* **2010**, *45*, 3497–3505. [[CrossRef](#)]
4. Yao, H.; You, Z.; Li, L.; Goh, S.W.; Lee, C.H.; Yap, Y.K.; Shi, X.M. Rheological properties and chemical analysis of nanoclay and carbon microfiber modified asphalt with Fourier transform infrared spectroscopy. *Constr. Build. Mater.* **2013**, *38*, 327–337. [[CrossRef](#)]
5. Zhang, H.; Zhu, C.; Tan, B.; Shi, C. Effect of organic layered silicate on microstructures and aging properties of styrene-butadiene-styrene copolymer modified bitumen. *Constr. Build. Mater.* **2014**, *68*, 31–38. [[CrossRef](#)]
6. Abdelrahman, M.; Katti, D.R.; Ghavibazoo, A.; Upadhyay, H.B.; Katti, K.S. Engineering physical properties of asphalt binders through nanoclay-asphalt interactions. *J. Mater. Civ. Eng.* **2014**, *26*, 1–9. [[CrossRef](#)]
7. Nazzal, M.D.; Kaya, S.; Gunay, T.; Ahmedzade, P. Fundamental characterization of asphalt clay nanocomposites. *J. Nanomech. Micromech.* **2013**, *3*, 1–8. [[CrossRef](#)]
8. Goh, S.W.; Akin, M.; You, Z.; Shi, X. Effect of deicing solutions on the tensile strength of micro- or nano-modified asphalt mixture. *Constr. Build. Mater.* **2011**, *25*, 195–200. [[CrossRef](#)]
9. Fang, C.; Yu, R.; Liu, S.; Li, Y. Nanomaterials applied in asphalt modification: A review. *J. Mater. Sci. Technol.* **2013**, *29*, 589–594. [[CrossRef](#)]
10. Li, R.; Xiao, F.; Amirkhani, S.; You, Z.; Huang, J. Developments of nano materials and technologies on asphalt materials—A review. *Constr. Build. Mater.* **2017**, *143*, 633–648. [[CrossRef](#)]
11. Zare-Shahabadi, A.; Shokuhfar, A.; Ebrahimi-Nejad, S. Preparation and rheological characterization of asphalt binders reinforced with layered silicate nanoparticles. *Constr. Build. Mater.* **2010**, *24*, 1239–1244. [[CrossRef](#)]
12. Li, R.; Pei, J.; Li, X.; Guo, Q. Preparation, mechanical and electric properties of polypropylene fiber reinforced lead zirconate titanate flexible materials. *Ferroelectrics* **2019**, *540*, 162–178. [[CrossRef](#)]
13. Li, P.; Li, Y.L. Review on Nano Modified Asphalt. *Appl. Mech. Mater.* **2014**, *587*, 1220–1223. [[CrossRef](#)]
14. Li, R.; Dai, Y.; Wang, P.; Sun, C.; Zhang, J.; Pei, J. Evaluation of nano-ZnO dispersed state in bitumen with digital imaging processing techniques. *J. Test. Eval.* **2018**, *46*, 974–983. [[CrossRef](#)]
15. Wang, H.P.; Gong, M.H.; Yang, J.; Niu, X.W. Advances in Nanometer Modified Asphalt. *Pet. Pitch* **2015**, *29*, 51–58.
16. Zhang, J.; Li, Z.; Li, M.; Xu, J.; Yin, W.; Liu, L. A study on mutual adaptability and mechanism of dispersion and stability of nanometer-modified asphalt. *Highway* **2005**, *8*, 142–146.
17. Ma, F.; Zhang, C.; Fu, Z. Performance & Modification Mechanism of Nano-CaCO₃ Modified Asphalt. *J. Wuhan Univ. Technol.* **2007**, *31*, 88–91.
18. Peplow, M. Nanoparticles go with the flow. *Nature* **2004**, *432*, 688.
19. Bourlinos, A.B.; Herrera, R.; Chalkias, N.; Jiang, D.D.; Zhang, Q.; Archer, L.A.; Giannelis, E.P. Surface-Functionalized Nanoparticles with Liquid-Like Behavior. *Adv. Mater.* **2005**, *17*, 234–237. [[CrossRef](#)]
20. Bourlinos, A.B.; Chowdhury, S.R.; Jiang, D.D.; Zhang, Q. Weakly solvated PEG-functionalized silica nanoparticles with liquid-like behavior. *J. Mater. Sci.* **2005**, *40*, 5095–5097. [[CrossRef](#)]
21. Bourlinos, A.B.; Giannelis, E.P.; Zhang, Q.; Archer, L.A.; Floudas, G.; Fytas, G. Surface-functionalized nanoparticles with liquid-like behavior: The role of the constituent components. *Eur. Phys. J.* **2006**, *20*, 109–117. [[CrossRef](#)] [[PubMed](#)]
22. Li, Q.; Dong, L.; Deng, W.; Zhu, Q.; Liu, Y.; Xiong, C. Solvent-free Fluids Based on Rhombohedral Nanoparticles of Calcium Carbonate. *J. Am. Chem. Soc.* **2009**, *26*, 9148–9149. [[CrossRef](#)] [[PubMed](#)]

23. Stulirova, J.; Pospisil, K. Observation of bitumen microstructure changes using scanning electron microscopy. *Road. Mater. Pavement* **2008**, *9*, 745–754. [[CrossRef](#)]
24. Puente-Lee, I.; Schabes-Retchkiman, P.S.; Rojas-García, J.; Ríos Guerrero, L.; Herrera-Nájera, R. Morphology of SBS-modified asphalt using low vacuum SEM. *Microsc. Microanal.* **2003**, *9*, 446–447. [[CrossRef](#)]
25. Zhang, H.; Chen, Z.; Xu, G.; Shi, C. Physical, rheological and chemical characterization of aging behaviors of thermochromic asphalt binder. *Fuel* **2018**, *211*, 850–858. [[CrossRef](#)]
26. Wei, J.; Liu, Z.; Zhang, Y. Rheological properties of amorphous poly alpha olefin (APAO) modified asphalt binders. *Constr. Build. Mater.* **2013**, *48*, 533–539. [[CrossRef](#)]
27. Zhang, H.; Chen, Z.; Xu, G. Evaluation of aging behaviors of asphalt binders through different rheological indices. *Fuel* **2018**, *221*, 78–88. [[CrossRef](#)]
28. Yang, X.; You, Z. High temperature performance evaluation of bio-oil modified asphalt binders using the DSR and MSCR tests. *Constr. Build. Mater.* **2015**, *76*, 380–387. [[CrossRef](#)]
29. Xing, X.Y.; Pei, J.Z.; Li, R.; Tan, X.Y. Effect and mechanism of calcium carbonate whisker on asphalt binder. *Mater. Res. Express.* **2019**, *6*, 055306. [[CrossRef](#)]
30. Cai, J.; Song, C.; Zhou, B.; Tian, Y.; Li, R.; Zhang, J.; Pei, J. Investigation on high-viscosity asphalt binder for permeable asphalt concrete with waste materials. *J. Clean. Prod.* **2019**, *228*, 40–51. [[CrossRef](#)]
31. Yao, H.; You, Z.; Li, L.; Goh, S.W.; Mills-Beale, J.; Shi, X.; Wingard, D. Evaluation of asphalt blended with low percentage of carbon micro-fiber and nanoclay. *J. Test. Eval.* **2013**, *41*, 278–288. [[CrossRef](#)]
32. Colbert, B.; You, Z. The properties of asphalt binder blended with variable quantities of recycled asphalt using short term and long term aging simulations. *Constr. Build. Mater.* **2012**, *26*, 552–557. [[CrossRef](#)]
33. Sui, C.; Farrar, M.J.; Tuminello, W.H.; Turner, T.F. New Technique for Measuring Low-Temperature Properties of Asphalt Binders with Small Amounts of Material. *Transp. Res. Rec. J. Transp. Res. Board* **2010**, *2179*, 23–28. [[CrossRef](#)]
34. Das, P.K.; Tasdemir, Y.; Birgisson, B. Low temperature cracking performance of WMA with the use of the Superpave indirect tensile test. *Constr. Build. Mater.* **2012**, *30*, 643–649. [[CrossRef](#)]
35. Yildirim, Y. Polymer modified asphalt binders. *Constr. Build. Mater.* **2007**, *21*, 66–72. [[CrossRef](#)]
36. Shen, J.; Amirkhanian, S.; Tang, B. Effects of rejuvenator on performance-based properties of rejuvenated asphalt binder and mixtures. *Constr. Build. Mater.* **2007**, *21*, 958–964. [[CrossRef](#)]
37. Lee, S.J.; Amirkhanian, S.N.; Park, N.W.; Kim, K.W. Characterization of warm mix asphalt binders containing artificially long-term aged binders. *Constr. Build. Mater.* **2009**, *23*, 2371–2379. [[CrossRef](#)]
38. ASTM. *Standard Test Method for Determining the Flexural Creep Stiffness of Asphalt Binder Using the Bending Beam Rheometer (BBR)*; ASTM Committee D04; ASTM: Madison, WI, USA, 2012.
39. Lei, Y.A.; Xiong, C.X.; Dong, L.J.; Guo, H.; Su, X.H.; Yao, J.L.; You, Y.J.; Tian, D.M.; Shang, X.M. Ionic liquid of ultralong carbon nanotubes. *Small* **2007**, *3*, 1889–1893. [[CrossRef](#)]
40. Du, Z.; Jia, Z.; Rao, G.; Chen, J. Study on surface properties of modified nanometer calcium carbonate. *Mod. Chem. Ind.* **2001**, *21*, 42–44.
41. Wang, Y.Z.; Chen, M.; Zeng, Z.Q. Modification Research Development on Nanometer Calcium Carbonate Surface. *Guangdong Chem. Ind.* **2008**, *35*, 42–45.

